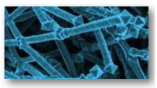
Materiales

Revista Mexicana de Ingeniería Química
Vol. 14, No. 3 (2015) 781-788

STRUCTURAL AND RAMAN SCATTERING STUDIES OF ZnO Cu NANOCRYSTALS GROWN BY SPRAY PYROLYSIS

ESTUDIOS ESTRUCTURALES Y DE DISPERSIÓN DE RAMAN DE NANOCRISTALES DE ZnO-Cu CRECIDOS POR SPRAY PIRÓLISIS

B. El Filali[1]*, T. V. Torchynska[2], A.I. Díaz Cano[1], M. Morales Rodriguez[1]
[1] *UPIITA-Instituto Politécnico Nacional, México D.F.07738, México.*
[2] *ESFM-Instituto Politécnico Nacional, México D.F.07738, México.*
Received October 29, 2014; Accepted May 21, 2015

Abstract
The paper presents a simple method to produce the ZnO nanocrystals (NCs) doped with Cu atoms by means of the spray pyrolysis using Zinc acetylacetonate hydrate, copper acetylacetonate and chloroform as solvent. ZnO nanocrystals with 5?20 wt % Cu were deposited on the glass substrates at 400°C using the spray pyrolysis technique and then thermal annealed at 500°C for 2 hours in ambient atmosphere. The crystallinity and morphology of the films were characterized by SEM, XRD and Raman scattering methods. The XRD study indicates that ZnO films have a hexagonal wurtzite structure and the Cu addition enhances the preferential orientation along the (1 0 0). The Raman scattering spectrum of Cu doped ZnO nanocrystals thermal annealed at 500°C for 2 hours in ambient atmosphere demonstrates a set of Raman peaks related to the vibrational modes in ZnO for small Cu concentration (5-10%). In ZnO nanocrystals with higher Cu concentrations (15-20%) the CuO phase was detected by the XRD and Raman scattering methods. It was shown that the quality of ZnO NC films can be improved by copper doping with concentration less than 10%.
Keywords: zinc oxide, SEM, XRD, Raman scattering.

Resumen
Este artículo presenta un método simple para producir nanoestructuras de ZnO con la inclusión de nanocristales metálicas de Cu por medio de spray pirolisis utilizando hidrato de acetilacetonato de zinc, acetilacetonato de cobre y cloroformo como disolvente. Las nanocristales de ZnO con un peso atómico de 5-20% de Cu se depositaron a una temperatura de 400°C sobre los sustratos de vidrio utilizando la técnica de spray pirolisis, después a las muestras se le aplico tratamiento térmico a 500°C en atmósfera ambiente. La cristalinidad y la morfología de las películas se caracterizaron por las técnicas de SEM, XRD y dispersión Raman. El estudio XRD indica que las películas de ZnO tienen una estructura de wurtzita hexagonal y que la adición de Cu mejora la orientación preferencial a lo largo de (1 0 0). El espectro de dispersión Raman de las muestras de ZnO dopadas con Cu después del tratamiento térmico a 500°C en atmósfera ambiente demuestran un conjunto de picos relacionados con los modos activos Raman de las nanopartículas de ZnO a niveles bajos de concentración de Cu (5-10%). En las nanocristales de ZnO con alta concentración de Cu (15-20%) se detectó la presencia de la fase secundaria de CuO por la técnica de difracción de rayos X. Además se demostró que la calidad de las nanopartículas de ZnO se puede mejorar con un nivel de dopaje con Cu inferior al 10%.
Palabras clave: óxido de zinc, SEM, XRD, la dispersión Raman.

1 Introduction

In the last decades, the zinc oxide nanocrystals (NCs) were investigated intensively owing to their important optical and electrical properties, as well as the possibility to be used in a great number of electronic applications, such as photodetectors, acoustic devices, thin film transistors, lasers, white light emitting diodes, mechanical and biomedical sensing nanodevices, sensors and actuators, solar cells,

* *Corresponding author. E-mail*: braelf@hotmail.com

high-density data storage devices, UV detectors etc (Javed *et al*, 2014; Kahraman *et al*, 2013). ZnO NC films are interesting as well for the application in photo catalysis, as transparent conducting and super hydrophobic materials, etc. (Tang *et al*, 2014; Tarwal *et al*, 2014; Torchynska, *et al*, 2014; Shinde *et al*, 2013). The majority of these applications of ZnO NCs are owing to a wide direct band gap of 3.37 eV and a large excitonic binding energy of 60 meV, as well as excellent physical, optical and electrical proprieties (Benharrats *et al*, 2010; Saidani *et al*, 2014). The characteristics of ZnO NCs can be modified by the impurity doping, such as aluminum, erbium, silver, gold, copper, etc... The ZnO doping with Cu has attracted an enormous attention recently due to the expected applications in light emitting diodes and magnetic semiconductors (Ghosh *et al*, 2009; Sahu *et al*, 2014).

Many techniques have been used to deposit the doped ZnO films, including CVD, sol-gel process and spray pyrolysis. Considering the different techniques, the spray pyrolysis is a simple method and its requirements are inexpensive. By using the spray pyrolysis technique, it is possible to produce the large area films, as well as multilayered or doped thin films.

Additionally the Cu doped ZnO NCs are interesting as a white light emission material, because Cu doping at some concentrations stimulates the light emission in the red-green-yellow spectral range, that permits to obtain white light in high quality ZnO NCs with efficient near band edge (blue) emission as well (El Filali *et al*, 2015). Furthermore, the Cu atoms, as expected, are suitable for obtaining the p-type ZnO material because the Cu atoms can replace of Zn atoms in the ZnO crystal lattice. The Cu atoms in the ZnO crystal lattice are considered as a deep acceptor which affects electrical and optical properties (Bae *et al*, 2014; Kamalianfar *et al*, 2014; Kim *et al*, 2009). A set of recent theoretical and experimental papers report that the Cu atoms substitute preferentially of Zn atoms and provoke a local magnetic moment in the ZnO crystal lattice as well (Xia *et al*, 2014). Thus the structural and optical studies of ZnO NCs doped by Cu atoms are of great interest owing to a necessity of the development of a simple technological method for their production with controllable optical properties.

2 Experimental details

The ZnO Cu nanocrystals were synthesized from the spraying chemical solution of the 0.1mol of high purity Zinc acetylacetonate hydrate ($Zn(C_5H_7O_2)_2$) (Aldrich) in chloroform, after keeping this solution for 30 min in the ultrasonic bath for the homogeneous component dissolution. The appropriate volume of copper acetylacetonate ($Cu(C_5H_7O_2)_2$) (Aldrich) was diluted in chloroform as well and added to a spray solution to obtain the doping Cu concentrations of 5, 10, 15 and 20 wt% in a spray solution. The resulting solution was sprayed with a rate of 7 ml/min, using a pneumatic spray set-up with a compressed air (10 LPM) as a carrier gas (Aklilu *et al*, 2013). The glass sheets with a size of 25 × 20 × 1 mm previously cleaned in an ultrasonic bath for 10 min were used as a substrate. The deposition temperature was fixed at 400°C for all samples, denoted as S1, S2, S3 and S4 with the Cu concentrations 5, 10, 15 and 20 wt.%, respectively. All samples were then thermal annealed at 500°C for 2 hours in ambient atmosphere.

The morphology and a crystal structure of ZnO NCs were characterized by the scanning electron microscopy (SEM) and X-ray diffraction (XRD) methods. The scanning electron microscopy JOEL-JSM7800F has been used (Soto *et al*, 2014). The XRD equipment of a model XPERT MRD with the detector Pixel, three axis goniometry and parallel collimator, with the resolution of 0.0001 degree has been applied. The X-ray beam was from the Cu source, Kα1 line λ=1.5406 A. Raman scattering spectra were measured in Jobin-Yvon Lab-RAM HR800 UV micro-Raman system using an excitation by a solid state light-emitting diode with a light wavelength of 532nm (Luna *et al*, 2013; Torchynska *et al*, 2008).

3 Results and discussion

3.1 SEM and XRD studies

SEM images of Cu doped ZnO NC films for different Cu concentrations after thermal annealing are presented in figure 1a-d. The size of ZnO NCs decreases with raising the Cu concentration in the films as it is shown in Table 1.

XRD results for the samples with different Cu concentrations are presented in figure 2. The annealing at 500°C for 2 hours in ambient air stimulates the process of ZnO oxidation and crystallization. The comparison of XRD peak positions with the available data base card no. 36-1451 shows that these peaks correspond to the X-ray diffraction from the (100), (002), (101), (102), (110), (103) and (112) crystal planes in the wurtzite ZnO crystal structure.

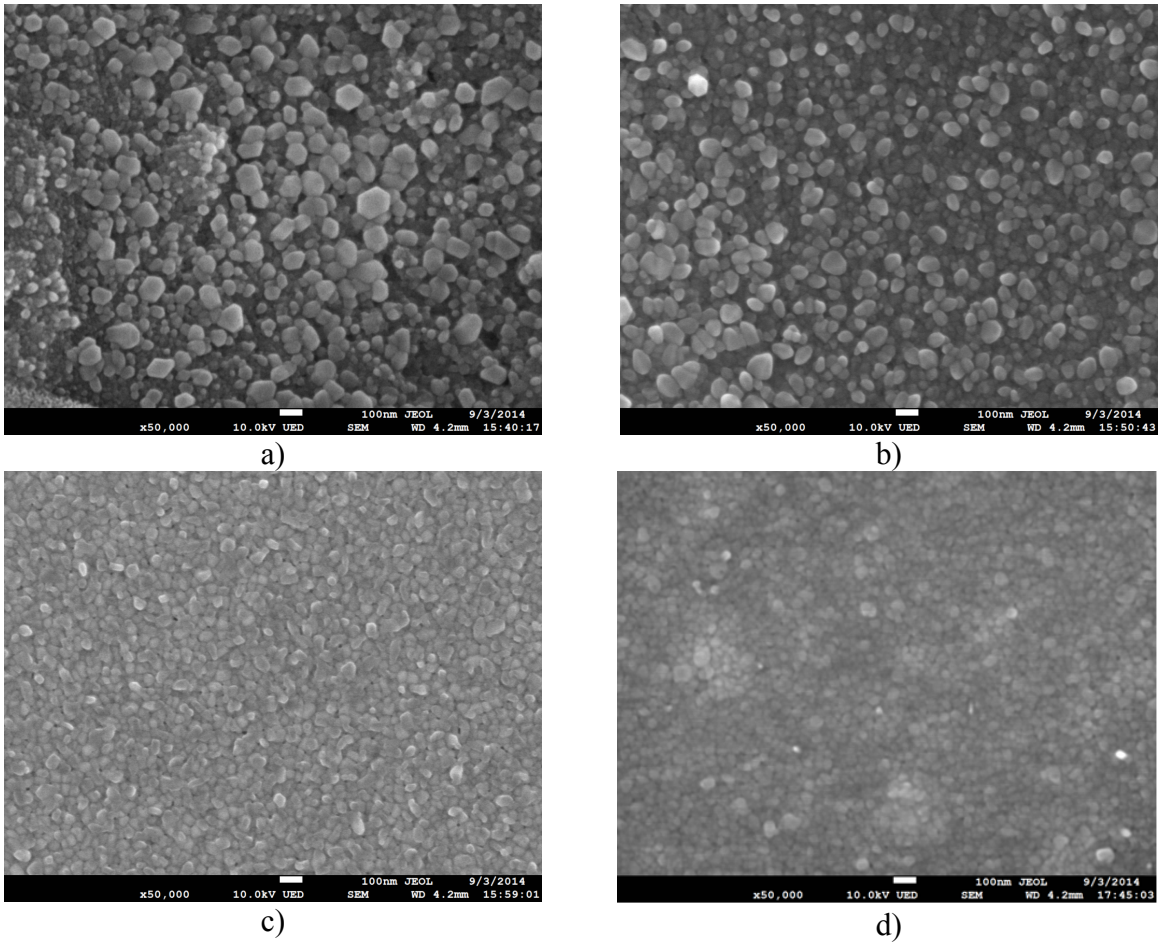

Fig. 1. SEM images of the spray deposited Cu doped ZnO thin films at various Cu concentration (a) S1, (b) S2, (c) S3 and (d) S4.

Table 1. The NC size variation versus Cu concentration

Samples	Cu concentration, %	The average NC size D estimated in SEM images, (nm)
S1	5%	96.2
S2	10%	81.4
S3	15%	54.6
S4	20%	22.3

When the Cu doping concentration increases, the position of the diffraction peaks shifts monotonically into the higher angle range (Figure 3, Table 2). In the samples S1 and S2 the second phase has not been detected, but in the samples S3 and S4 the second phase of CuO has been revealed as a peak at the angle 38.731o corresponding to the diffraction from the plane (111) in the monoclinic CuO crystal lattice (Fig.2).

The parameters of ZnO crystal lattices were calculated for all studied samples (Table 2) that reveals decreasing monotonically the ZnO crystal lattice parameters with Cu concentration rising in the films. Actually the both "red" and "blue" XRD peak shifts in ZnO Cu crystals in comparison with undoped ZnO were presented in the literature (Chowa *et al*, 2013; Kulyk *et al*, 2009; Ligang *et al*, 2011; Núñez *et al*, 2011;. Yan *et al*, 2006).

Table 2. XRD peaks and the wurtzite ZnO lattice parameters

Crystal planes	Bulk ZnO 2Θ (º) [ ]	S1, 5%Cu, 2Θ (º)	S2, 10%Cu, 2Θ (º)	S3, 15%Cu, 2Θ (º)	S4, 20%Cu, 2Θ (º)
(100)	31.770	31.897	32.040	32.331	32.439
(002)	34.440	34.607	34.786	35.077	35.051
(101)	36.253	36.377	36.628	36.811	36.847
"a"(Å)	3.2498	3.239	3.217	3.202	3.199
"c" (Å)	5.2066	5.189	5.154	5.130	5.125

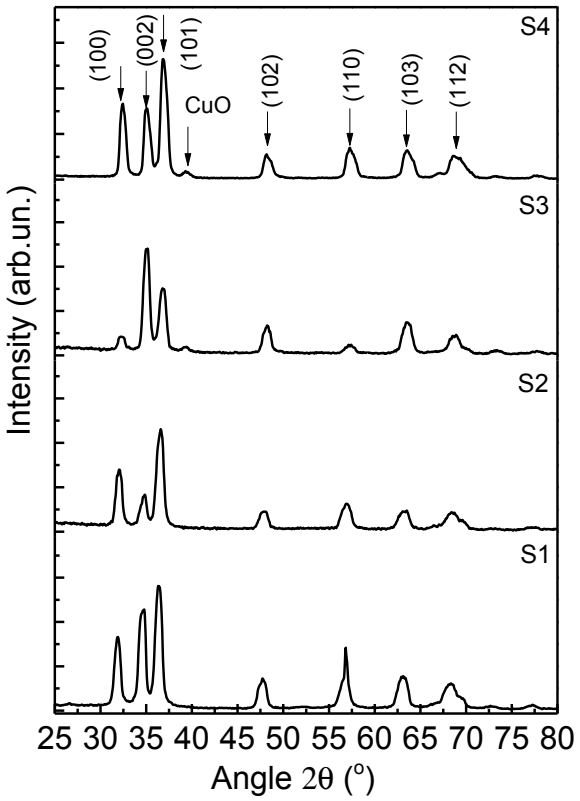

Fig. 2. XRD patterns of ZnO NC films with different Cu concentrations.

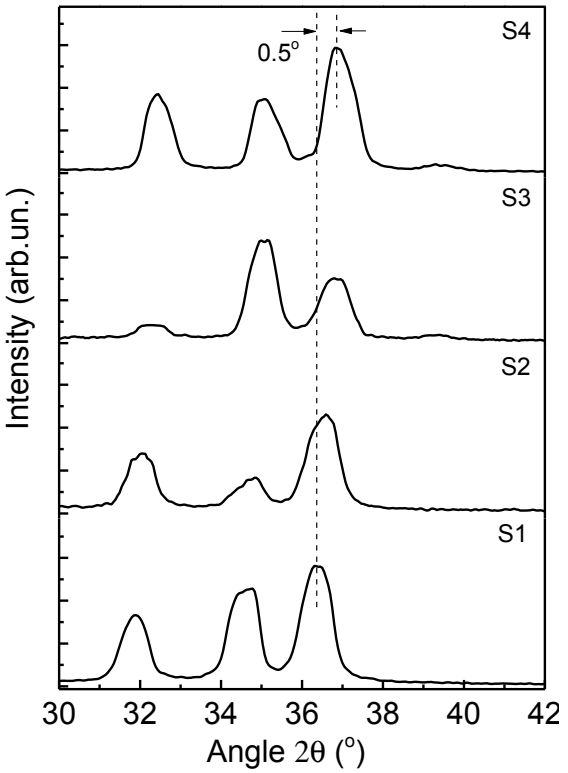

Fig. 3. The shift of XRD peaks in ZnO Cu NC films versus Cu concentrations.

Note that the valence of Cu could be +1 or +2 in the ZnO:Cu crystal lattice. The radius of Cu^{+}, Cu^{+2} and Zn^{+2} ions are 0.096, 0.072 and 0.074 nm, respectively. Thus the Cu^{+}, Cu^{+2} substitution ions and the Cu^{+2} interstitial ions might be the main impurities in ZnO:Cu NCs. The Cu defects would impact on the concentrations of interstitial Zn atoms, of Zn and oxygen vacancies as well (Peng *et al*, 2008). As Cu^{+} ions substituted Zn^{+2} ions in the crystal lattice, the increase of the lattice constant and inter planar distances will be realized, which would lead as well to decreasing the diffraction angles compared with undoped ZnO NCs. In contrary if Cu^{+2} ions substituted Zn^{+2} ions, the decrease of the lattice parameters and inter planar distances will be detected together with increasing the diffraction angles in XRD in comparison with undoped ZnO. Hence the decreasing monotonically the ZnO lattice parameters in studied samples at rising Cu concentrations in the range of 5-15% testifies that the Cu^{+2} ions substituted Zn^{+2} ions mainly for the studied Cu concentrations. At higher Cu concentration (20%) the variation of ZnO lattice parameters is negligible (Table 2), but the second phase CuO is detected additionally in studied films.

Table 3. Raman scattering spectrum analysis

Samples	E_2 (low) (cm^{-1})	*Raman Active Modes of CuO*			$3E_{2H}$-E_{2L} (cm^{-1})	A_1 (TO) (cm^{-1})	E_1 (TO) (cm^{-1})	E_2 (High) (cm^{-1})	A_1 (LO) (cm^{-1})	E_1 (LO) (cm^{-1})
		A_g(cm^{-1})	B_g^1(cm^{-1})	B_g^2(cm^{-1})						
Bulk ZnO [31]	101	---	---	---	---	380	407	437	574	583
Bulk CuO [30]	---	296	344	628	---	---	---	---	---	---
S1	100.9	---	---	---	333	---	---	439.6	---	585
S2	101	---	---	---	333	---	---	437.8	---	581.5
S3	101	298.6	348.5	---	---	---	---	440.0	---	584
S4	100.5	293.5	343.3	---	---	---	---	439.5	---	583.3

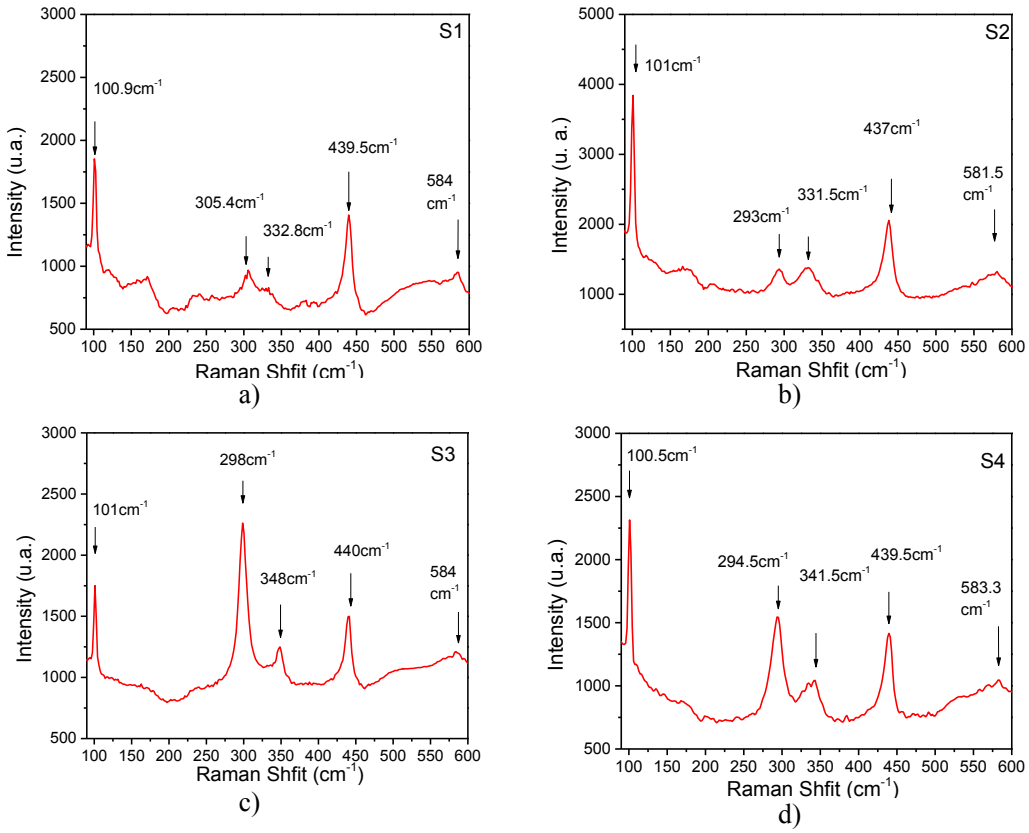

Fig. 4. Raman scattering spectra of ZnO NC films obtained at different Cu concentrations: 5 (a), 10 (b), 15 (c) and 20% (d).

3.2 Raman scattering study

Raman scattering spectra have been measured for the films in order to study how the different Cu atom concentrations change the Raman scattering of ZnO NC films. These ZnO films have a wurtzite structure with C_{6V}^4 point group symmetry (Lupan *et al*, 2011):

$$\Gamma_{opt} = A_1 + 2B_1 + E_1 + 2E_2 \quad (1)$$

The group theory predicts that the ZnO structures present the Raman active optic phonons in Brillouin zone center such as: A_1 and E_1 symmetry polar

phonons with different frequencies, transversal optic-(TO) and longitudinal optic-(LO) phonons, and E_2 - a symmetry non-polar phonon mode with the frequencies E_{2L} and E_{2H}. The B1 modes are infrared and Raman inactive modes. The E_{2H} (high) mode is associated with the oxygen sublattice, also it is characteristic of the wurtzite phase material. The E_{2L} (low) mode is attributed to the Zn sublattice (Ashkenov *et al*, 2003; Lupan *et al*, 2011; Torchynska *et al*, 2014). Raman peak at 100.5-101.0 cm^{-1} detected in studied Cu doped ZnO NCs after thermal annealing (Figure 4) can be attributed to the first order Raman peak in the wurtzite crystal lattice related to E_{2L}. The Raman peak at 333 cm^{-1} (Figure 4, Table 3) was attributed to the second order Raman peak arising from the zone boundary phonon $3E_{2H} - E_{2L}$. The Raman peaks 437-440 cm^{-1} and 582-584 cm^{-1} (Figure 4, Table 3) were attributed to the E_{2H} mode and E_1 LO phonon mode in ZnO NCs (Torchynska *et al*, 2014). It is clear in figure 5, that the intensity of E_{2L} and E_{2H} Raman non-polar phonon modes increase with the copper concentration until 10%, and then starts decreasing when the copper concentration increases. This fact indicates that the quality of ZnO NC films can be improved with the copper concentration not more than 10%.

CuO has been characterized by a monoclinic crystal structure and it belongs to space group symmetry of C_{2h}^6 (Diaz *et al*, 2013). There are twelve zone center optical phonon modes defined by 4Au+5Bu+Ag+2Bg; and three of them (Ag+2Bg) are Raman active (Yu *et al*, 2004). The peaks shown in the figure 4 at 296-305.4cm^{-1} and 343-348cm^{-1}, are attributed to the Ag and B_g^1 active Raman modes in the CuO monoclinic phase, respectively (Chrzanowski *et al*, 1989; Diaz *et al*, 2013; Yu *et al*, 2004).

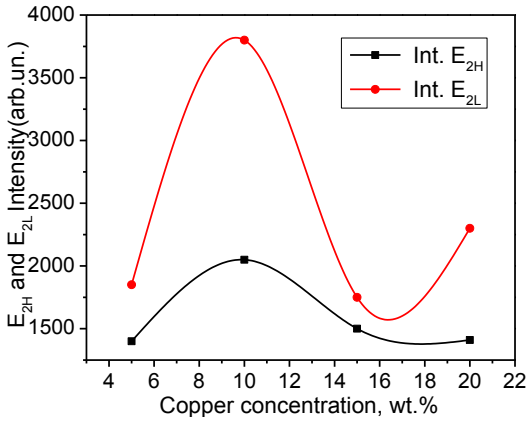

Fig. 5. The E_{2L} and E_{2H} Raman mode intensity variation versus Cu concentration.

Conclusions

Cu doped ZnO nanocrystals have been prepared by the spray pyrolysis method with follows thermal annealing. The X-ray diffraction study shows that the introduction of Cu atoms in the ZnO wurtzite crystal lattice was achieved, which causes decreasing the ZnO lattice parameters. Additionally in the samples S3 and S4 the second monoclinic phase of CuO has been detected in the XRD pattern and Raman scattering spectra. SEM study reveals decreasing the ZnO NC average size from 96.2 nm down to 22.3 nm with rising Cu concentration. It was shown that the quality of ZnO NC films can be improved by copper doping with concentration less than 10%.

Acknowledgement

The authors would like to thank SIP-IPN, Mexico, for the financial support, as well as the CNMN-IPN for Raman, SEM and XRD measurements, and special thanks for the Lic. Leticia Oviedo for her technical help.

References

Ashkenov, N., Mbenkum, B.N., Bundesmann, C., Riede, V., Lorenz, M., Spemann, D., Kaidashev, E.M., Kasic, A., Schubert, M., Grundmann, M., Wagner, G., Neumann, H., Darakchieva, V., Arwin, H. and Monemar, B. (2003). Zinc Oxide Bulk, Thin Films and Nanostructures. *Journal of Applied Physics 93*, 126.

Aklilu, M. and Tai, Y. (2013). Self-assembled monolayers assisted thin film growth of aluminum doped zinc oxide by spray pyrolysis method. *Applied Surface Science 270*, 648-654.

Bae, H.Y. and. Choi, G. M (1999. Electrical and reducing gas sensing properties of ZnO and ZnO-CuO thin films fabricated by spin coating method. *Sensors and Actuators, B55*, 47-54.

Benharrats, F., Zitouni, K., Kadri, A. and Gil, B. (2010). Determination of piezoelectric and spontaneous polarization fields in Cd_xZn_{1-x}/ZnO quantum wells grown along the polar (0001) direction. *Superlattices Microstructures 47*, 592-596.

Chowa, L., Lupana, O., Chaia, G., Khallaf, H., Ono, L.K., Roldan, C.B., Tiginyanu, I.M.,

Ursaki, V.V., Sontea, V. and A. Schulte. (2013). Synthesis and characterization of Cu-doped ZnO one-dimensional structures for miniaturized sensor applications with faster response. *Sensors and Actuators A 189*, 399-408

Chrzanowski, J. and Irwin, J.C (1989). Raman scattering from cupric oxide. *Solid State Communications 70*, 11-14.

Diaz, C.A.I., El Filali, B., Torchynska, T.V. and Casas, E.J.L. (2013). Structure and emission transformations in ZnO nanosheets at thermal annealing. *Journal of Physics and Chemistry of Solids 74*, 431-435

Diaz, C.A.I., El Filali, B., Torchynska, T.V. and Casas, E.J.L. (2013). ??White?? emission of ZnO nanosheets with thermal annealing. *Physica E 51*, 24-28.

Dojalisa, S., Panda, N.R. Acharya, B.S. and Panda, A.K. (2014). Microstructural and optical investigations on sonochemically synthesized Cu doped ZnO nanobricks. *Ceramics International 40*, 11041-11049.

El Filali B., Torchynska, T.V. and Diaz Cano, A.I. (2015). Photoluminescence and Raman scattering study in ZnO:Cu nanocrystals. *Journal of Luminescence 161*, 25-30.

Ghosh, T., Dutta, M., Mridha, S. and Basak, D. (2009). Effect of Cu doping in the structural, electrical, optical, and optoelectronic properties of sol-gel ZnO thin film. *Journal of the Electrochemical Society 156*, H285.

Iqbal, Javed, Tariq, J., Shafiq, M., Arshad, A., Naeem, A., Saeed, B. and Ronghai. B. (2014). Synthesis as well as Raman and optical properties of Cu-doped ZnO nanorods prepared at low temperature. *Ceramics International 40*, 2091-2095

Kahraman, S., Cakmak, H.M., Cetinkaya, S., Bayansal, F., Cetinkara, H.A. and Guder, H.S. (2013). Characteristics of ZnO thin films doped by various elements. *Journal of Crystal Growth 363*, 86-92.

Kamalianfar, A., Halim, S.A., and ak, A.K. (2014). Synthesis of ZnO/Cu micro and nanostructures via a vapor phase transport method using different tube systems. *Ceramics International 40*, 3193-3198.

Kim, G.H., Kim, D .L, Ahn, B. D., Lee, S. Y. and Kim, H. J. (2009). Investigation on doping behavior of copper in ZnO thin film. *Microelectronics Journal 40*, 272.

Kulyk, B., Sahraoui, B., Figà, V., Turko, B., Rudyk, V. and Kapustiansky, A. (2009). Effect of Cu on the microstructure and electrical properties of Cu/ZnO thin films. *Journal of Alloys Compounds 481*, 819-825

Ligang, Ma., Shuyi, Ma., Haixia, C., Xiaoqian and A., Xinli H. (2011). Microstructures and optical properties of Cu-doped ZnO. *Applied Surface Science 257*, 10036-10041

Luna, S. R.A., Zermeño, R.B.B., Moctezuma, E., Contreras, B. R.E., Leyva1, E. and López B.M.A. (2013). Photodegradation of omeprazole in aqueous solution using TiO_2 as catalyst. *Revista Mexicana de Ingeniería Química 12*, 85-95.

Lupan, O., Pauporte,T., Viana, B. and Aschehoug, P. (2011). Electrodeposition of Cu-doped ZnO nanowire arrays and heterojunction formation with p-GaN for color tunable light emitting diode applications. *Electrochimica Acta 56*, 10543-10549.

Núñez, S.M.C., García-Suarez, F.J., Gutierrez, M.F.M., Sánchez, R. M. and Bello, P.L.A.(2011). Some intrinsic and extrinsic factors of acetylated starches: morphological, physicochemical and structural characteristics. *Revista Mexicana de Ingeniería Química 10*, 501-512.

Peng, X., Xu, J.and Zang. X. (2008). Structural and PL properties of Cu-doped ZnO films. *Joural of Luminescence 128*, 297

Saidani, T., Zaabat, M., Salah, M.A., Ben aboud, A., Benzitouni, S. and Azzedine Boudine. (2014). Influence of annealing temperature on the structural, morphological and optical properties of Cu doped ZnO thin films deposited by the sol-gel method. *Superlattices and Microstructures 75*, 47-53.

Shinde, S.S., Bhosale, C. H. and Rajpure, K. Y. (2013). Photo electrochemical proper- ties

of highly mobilized Li-doped ZnO thin films. *Journal of Photochemistry and Photobiology B. Biology 120*, 1-9.

Soto, B.M.A., Sánchez C. V.M and Trujillo, C.M.E.. (2014). Caracterización de películas serigrafías de TiO_2/alginato. *Revista Mexicana de Ingeniería Química 13*, 227-236.

Tang, L., Yang, S., Wang, Z. and Zhou, B. (2013). Synthesis of hydrophobic ZnO branches by phase transfer-based solution method. *Ceramics International 39*, 5771-5776.

Tarwal, N.L., Gurav, K.V. and Mujawar, S.H. (2014). Photoluminescence and photoelectrochemical properties of the spray deposited copper doped zinc oxide thin films. *Ceramics International 40*, 7669-7677.

Torchynska T.V., Douda, J., Ostapenko, S.S., Jimenez-Sandoval, S. Phelan, C., Zajac, A., Zhukov, T. and Sellers, T. (2008). Peculiarities of Raman scattering in bioconjugated CdSe/ZnS quantum dots. it Journal of Non-Crystaline Solids 354, 2885.

Torchynska, T. V. and El Filali, B. (2014). Size dependent emission stimulation in ZnO nanosheets. *Journal of Luminescence 149*, 54-60.

Xia, C., Wang, F. and Hu, C. (2014). Theoretical and experimental studies on electronic structure and optical properties of Cu-doped ZnO. *Journal of Alloys and Compounds 589*, 604-608.

Yan, Y., M.M. Al-Jassim, S.H. Wei. (2006). Doping of ZnO by group-IB elements. *Applied Physics Letters 89*, 181912

Yu, T., Zhao, X., Shena, Z.X., Wu, Y.H. and Su, W.H. (2004). Investigation of individual CuO nanorods by polarized micro-Raman scattering. *Journal of Crystal Growth 268*, 590-595.